Molecular Crystals and Liquid Crystals

ISSN: 1542-1406 (Print) 1563-5287 (Online) Journal homepage: http://www.tandfonline.com/loi/gmcl20

Gaussian Distribution of the Charge Traps in the Energy Gap of MDMO-PPV and Its Dependence on Synthesis Route Revealed by the Thermally Stimulated Current Spectroscopy

M. Pranaitis, A. Sakavičius, V. Janonis & V. Kažukauskas

To cite this article: M. Pranaitis, A. Sakavičius, V. Janonis & V. Kažukauskas (2014) Gaussian Distribution of the Charge Traps in the Energy Gap of MDMO-PPV and Its Dependence on Synthesis Route Revealed by the Thermally Stimulated Current Spectroscopy, Molecular Crystals and Liquid Crystals, 604:1, 96-106, DOI: 10.1080/15421406.2014.968037

To link to this article: http://dx.doi.org/10.1080/15421406.2014.968037

Published online: 15 Dec 2014.

Mol. Cryst. Liq. Cryst., Vol. 604: pp. 96–106, 2014

ISSN: 1542-1406 print/1563-5287 online
DOI: 10.1080/15421406.2014.968037

Gaussian Distribution of the Charge Traps in the Energy Gap of MDMO-PPV and Its Dependence on Synthesis Route Revealed by the Thermally Stimulated Current Spectroscopy

M. PRANAITIS, A. SAKAVIČIUS, V. JANONIS, AND V. KAŽUKAUSKAS*

Department of Semiconductor Physics and Institute of Applied Research of Vilnius University, Vilnius, Lithuania

Energetical distribution of the charge traps was investigated in MDMO-PPV ([poly-(2-methoxyl),5-(3,77dimethyloctyloxy)] paraphenylenevinylene). The thermally stimulated current spectroscopy was applied as a direct photoelectrical method immediately related with charge transport and trapping in materials with defect states. Possibility of the selective trapping states filling by the light with different spectra below and above the band gap was demonstrated. The analysis revealed the Gaussian distribution of the traps in the energy gap. The sensitivity of the technique is evidenced by the results, indicating that in MDMO-PPV synthesized by different routes – Gilch and Sulfinyl – different defect states were identified.

Keywords: MDMO-PPV; trapping states; photoconductivity; thermally stimulated currents

I. Introduction

Electrical properties of organic semiconductors are critically influenced by the charge transport and trapping phenomena, meaning that namely these phenomena are decisive factors conditioning the overall performance of the devices. Trapping states in disordered materials affect device performance in several ways. The most important issue is that they diminish the effective carrier mobility, and cause the imbalance of different carrier flows. In photoelectrical devices traps might create the nonradiative recombination centers, resulting in decrease of luminescence [1]. Hence, increase of the operating voltage reduces the operation stability of devices, and may lead to material degradation via solid-state electrochemical reactions [2–4]. Therefore, screening of defect states and their distribution is of key importance for controlling electrical properties of the material in order to understand and to optimize charge transport in devices.

*Address correspondence to V. Kažukauskas, Department of Semiconductor Physics and Institute of Applied Research of Vilnius University, Saulėtekio al. 9, Bldg. 3 LT-10222, Vilnius, Lithuania. E-mail: vaidotas.kazukauskas@ff.vu.lt

Color versions of one or more of the figures in the article can be found online at www.tandfonline.com/gmcl.

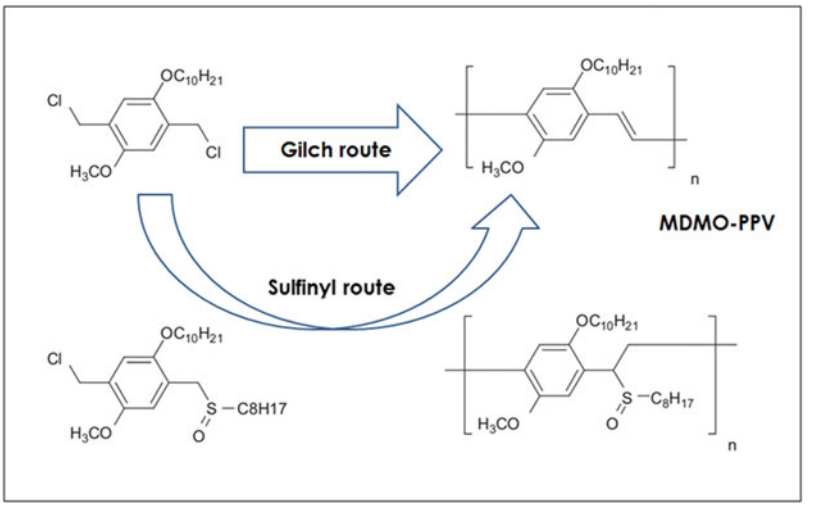

Figure 1. Gilch and Sulfinyl synthesis routes of MDMO-PPV.

Charge trapping in disordered organic semiconductors is generally described as thermally activated hopping in a Gaussian distribution of localized states [5]. One of the direct ways to investigate energetic distribution of traps are thermally stimulated methods [6–9]. Thermally Stimulated Current (TSC) technique is particularly efficient in determination of trap parameters in organic semiconductors because of the charge measurement principle. In fact, because of the low carrier mobilities, the relaxation process is much slower in organic materials than in conventional semiconductors, and measurement of the released charges is well adapted to such materials. The TSC method was proven to be a sensitive tool enabling to reveal, e.g., differences caused by polar molecular orientation in the films [10]. Moreover, it enabled to prove that trapping states, depending on their densities might act as transport states, governing in this way the whole charge transport in materials and devices [11] In this study, alongside with the integral TSC mode, we had adopted also the fractional heating TSC technique as a direct photoelectrical method to analyze distribution of trapping states in [poly-(2-methoxyl),5-(3,77dimethyloctyloxy)] paraphenylenevinylene (MDMO-PPV) synthesized in two different ways. MDMO-PPV is one of the promising conjugated polymers for organic solar cells due to ease of its processability as well as tunability of the optical and electronic properties through chemical modifications [12]. MDMO-PPV demonstrates excellent solubility in many organic solvents [13] and shows great performance in optoelectrical devices [14].

II. Samples and Experiment

The investigated MDMO-PPV polymers were synthesized in two different ways. Two popular synthesis routes are the Gilch and the Sulfinyl ones. They are showed in Fig. 1.

Gilch route is a dehydrohalogenation process which uses a dichloro-substituted monomer [15, 16]. Meanwhile the Sulfinyl route utilizes an asymmetric chloro-, sulfinyl-substituted monomer [17, 18]. The asymmetry in the sulfinyl monomer leads to a higher

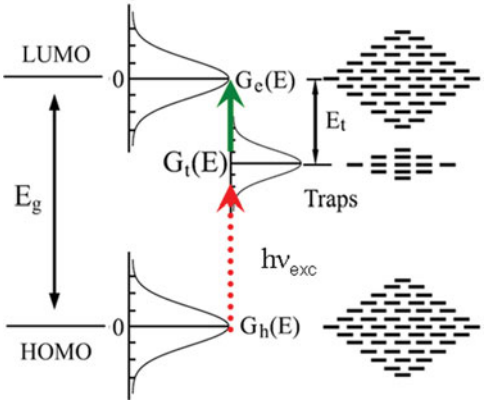

Figure 2. Energy levels with distributed states. $G_e(E)$ and $G_h(E)$ are the Gaussian densities of states for electrons and holes. The energy levels of traps within the energy gap (only electron traps are shown). E_t is the trap depth, $G_t(E)$ the density of states of the traps [21]. In such model our approach assures that carriers can be excited to different traps depending on the energy of the exciting light quanta $h\nu_{exc}$ (red dotted arrow). Afterwards upon heating carriers become thermally extracted with different thermal activation energies depending on which traps are filled (green arrow).

regularity in the polymer due to less head-to-head or tail-to-tail additions during polymerization. Thus, MDMO-PPV produced by the Sulfinyl method constitutes fewer defects that may act as trap sites than regular Gilch material [19]. The films were produced by the drop-casting on the Indium-Tin-Oxide (ITO) glass. ITO is used as the hole-injecting contact. The thickness of the films was about 1 μm. The Al electrode was evaporated on the top in a high vacuum.

The TSCs were measured in the temperature region from 77 K up to 350 K. The bias was supplied and current was measured by the source-measure unit Keithley 6430.The strength of the electrical field over the samples was 1×10^5 V/cm. The dark currents at the same bias were measured too and subtracted from the TSC data obtained after the light excitation. To scan the TSCs the traps were initially optically filled at 77 K by the focused light of the 100 W halogen lamp passed through the color filters. Ten long-pass color filters with cut-on energies ranging from 1.77 eV up to 3.1 eV were used. As LUMO band of MDMO-PPV is located at -2.8 eV and HOMO appears at -5 eV [20], in this way the selective excitation of trapping states in the band gap as well as the inter-band excitation of MDMO-PPV could be achieved. This is schematically demonstrated in Fig. 2. Within the framework of the model [21] our approach assures that carriers can be excited to different traps depending on the energy of the exciting light quanta. Afterwards upon heating carriers become thermally extracted with different effective thermal activation energies depending on which traps are filled.

After the light excitation, before starting the temperature scan, the sample was kept in the dark at liquid nitrogen (LN) temperature to assure the thermalization of carriers and filling of the trapping states (usually for more than 600 s). The standard heating rate was 10 K/min.

To analyze TSC spectra in detail and to gain information about the trap distribution we employed the informative repetitive heating mode, which enables analysis of the closely located trapping centers. The fractional TSC spectra were measured by using temperature

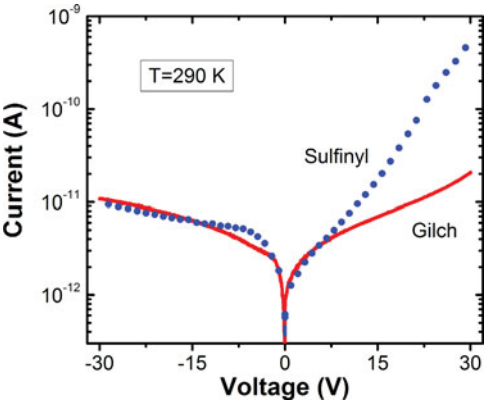

Figure 3. Current-voltage characteristics at 290 K of two MDMO-PPV samples synthesized in different ways.

intervals of $\Delta T = 10$ K. To obtain the set of the effective activation energy values, describing distribution of the trapping states, each trace measured by the multiple heating was fitted numerically by the following equation [6]:

$$I(T) = N_t e \mu \tau \nu_0 \left(\frac{U}{L}\right) \exp\left[-\frac{E_t}{kT} - \frac{\nu_0 k T^2}{\beta(E_t + kT)} \exp\left(-\frac{E_t}{kT}\right)\right] \quad (1)$$

Here E_t is the thermal trap activation energy, N_t is the density of trapped charge, e is the elementary charge, μ is carrier mobility, τ is the recombination lifetime, ν_0 is the carrier attempt-to-escape frequency, U is the applied electric field strength, A is the area of the sample, L is its thickness, k is the Boltzmann constant and T is the temperature. By fitting experimental data, the values of E_t, N_t, and ν_0 were used as fitting parameters.

The filling of the traps could be evaluated by integrating the experimental curves over time, according to the equation:

$$n_0 = \frac{Q}{ALeG}. \quad (2)$$

Here Q is the amount of charge released during the TSC experiment. It was calculated by integrating experimental curves over time. G is the photoconductivity gain.

III. Results and Discussion

First, current–voltage (I-V) tests of the samples prepared by the Gilch and Sulfinyl synthesis routes were done at room temperature. The dependencies are shown in Fig. 3. The samples synthesized by the Gilch route showed lower conductivity in the forward direction. This current decrease can be attributed to the presence of more trapping and/or recombination states as will be analyzed below. I-V characteristics measured in the reverse direction were similar, confirming that the electrical current trough the sample is controlled by the Al/MDMO-PPV contact potential barrier.

The TSC measurements were used as direct photoelectrical method to prove distribution of the trapping states in synthesized polymers. The characteristic behavior of the TSCs depending on the excitation cut-on energy in the Gilch sample is presented in Fig. 4. First of

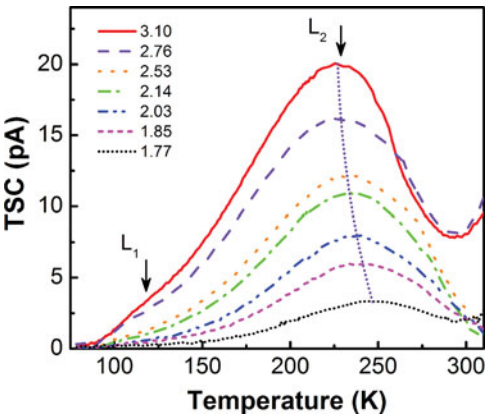

Figure 4. Set of TSC spectra in the Gilch sample depending on the excitation cut-on energies of the long-pass color filter, as indicated on figure. Arrows mark positions of two maxima (the first one is seen as a shoulder on the background of the growing current). Dotted violet line indicates shift of the maximum position of different curves.

all appearance of two maxima, characterizing different traps can be seen. They are marked by the arrows. The TSCs exhibit a main broad TSC peak at about 240 K (L_2) as well as a shoulder at about 120 K (L_1), indicating two different trap distributions. Moreover, the second peak demonstrates the shift towards the lower temperatures by increasing quantum energy. This indicates variation of the distribution of density of states (DOS) within the bandgap.

To analyze it in detail and to gain information about the trap distribution we employed the informative repetitive heating mode, which enables analysis of the closely located trapping centers. Figure 5 shows the set of the fractional TSC spectra recorded by using temperature intervals of $\Delta T = 10$ K. The gradual increase of the activation energies with temperature without any plateaus indicates a continuous trap distribution instead of discrete trap levels [22], as it was already expected on the basis of the broad TSC spectrum.

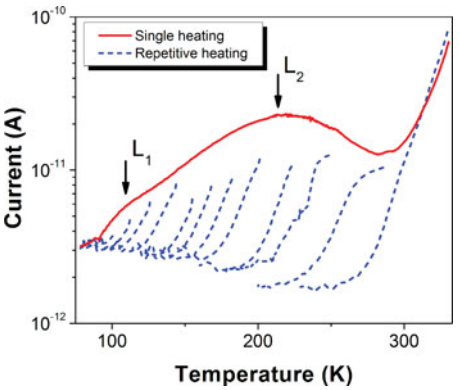

Figure 5. TSC spectra of the sample synthesized by the Gilch route obtained during single heating (conventional TSC), and the set of curves measured by repetitive heating.

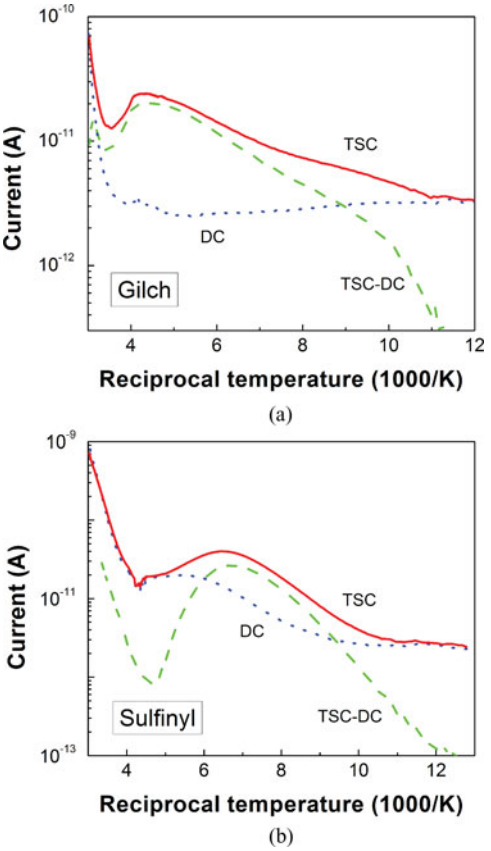

Figure 6. Experimental TSC spectra measured after the light excitation (TSC), dark currents (DC), and their differences (TSC-DC) in the samples synthesized by the Gilch (a) and the Sulfinyl (b) routes.

TSC curves for both synthesized polymers with and without subtracted dark currents are depicted in Fig. 6.

The shapes of both TSC spectra, i.e., broad maxima extended in wide temperature regions, indicate trap distribution instead of the discrete trap levels, implying that there is no single specific structural defect responsible for the trap creation. Moreover, clear differences in TSC spectra in both materials are seen, indicating different defect distribution. At the highest temperatures above 250 K other thermal generation process with higher activation energy becomes prevailing, such as the carrier pair band-to-band generation or carrier jumps over the barrier of metal contact, as seen in Fig. 6. Its influence starts masking that of the generation from the trap L_2, making it difficult to assess it.

To obtain the set of the effective activation energy values, describing distribution of the trapping states, each trace measured by the multiple heating (see Fig. 5) was fitted numerically by Eqs. (1), (2). The obtained distribution of the densities of the filled trapping states depending on the activation energies are presented in Fig. 7.

The distribution of the filled trapping states is rather broad. The histogram demonstrates a continuous trap distribution with activation energies varying between about 150 meV and 450 meV and two maxima at about 220 meV and 380 meV, representing two different traps

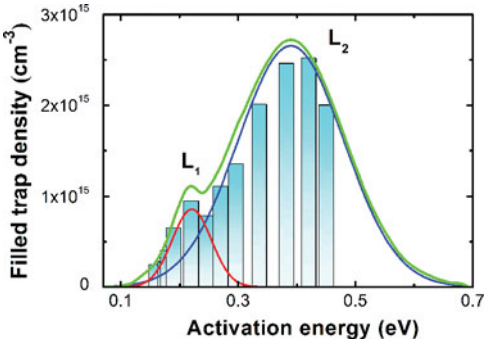

Figure 7. Filled trapping state density vs. activation energy of the sample synthesized by the Gilch route. L_1 and L_2 present the maximum position of two different traps levels.

(L_1, L_2). The distribution of the densities of the states follow the Gaussian distribution *G(E)*:

$$G(E) = \frac{N_t}{\sigma\sqrt{2\pi}} \exp\left[-\frac{(E - E_t)^2}{2\sigma^2}\right]. \quad (3)$$

Here E_t is the mean value of the trapping states level, σ is the standard deviation representing the width of the distribution. The experimental data were approximated by the Gaussian distribution function with the following parameters: $\sigma_1 = 25$ meV and $N_{t1} = 1.2 \times 10^{15}$ cm^{-3}, $\sigma_2 = 90$ meV and $N_{t2} = 2.7 \times 10^{15}$cm^{-3} (two single maxima in Fig. 7). These two traps might result from structural defects, as, e.g. chain ends and irregularities of the polymer layer.

Therefore, basing on these results the TSC curves were fitted by equation, which takes into account distribution of the trapping states in energy scale [23]:

$$I(T) = N_t e\mu\tau\nu_0 \left(\frac{A \cdot U}{L}\right) G(E) \cdot \exp\left(-\frac{E_t}{kT}\right) \exp\left[-\frac{\nu_0}{\beta}\int_{T_0}^{T} \exp\left(-\frac{E_t}{kT'}\right) dT'\right], \quad (4)$$

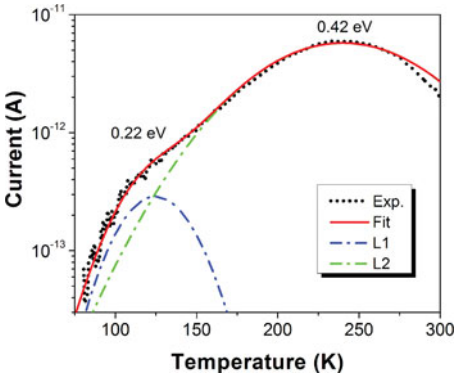

Figure 8. Example of the fitting of experimental TSC of the sample synthesized by the Gilch route. Dotted line shows experimental data, solid curve is fitting results, dash-dotted lines represent thermal generation of carriers from trapping states.

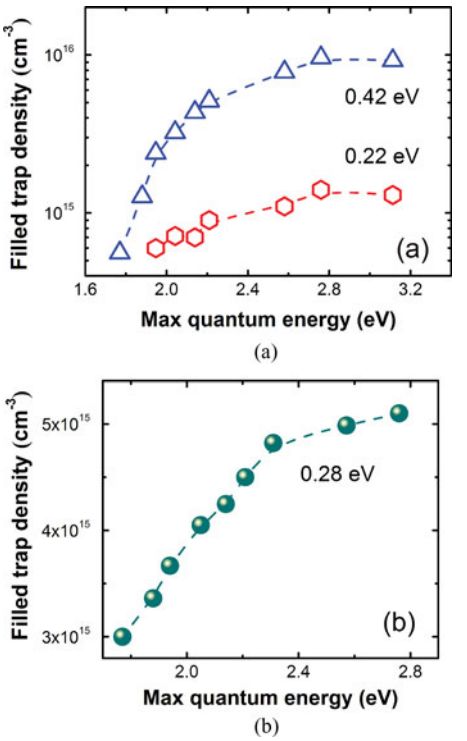

Figure 9. Density of the filled trapping states depending on the exciting light spectral edge in the samples synthesized by the Gilch (a), and Sulfinyl routes (b).

To limit the number of the fitting parameters, the initial density of the filled traps N_t was determined according to Eq. (2) and the attempt to escape frequency ν_0 was evaluated from the following relationship [24, 25]:

$$\nu_0 = 3\beta \left(\frac{T_m T'}{T_m - T'} \right) \exp \left(\frac{E_t}{kT_m} \right). \tag{5}$$

Here T' is the temperature at the half of the maximum current value on the low temperature side of the current peak. The trap is characterized by the maximum of the thermally stimulated current spectra appearing at the temperature T_m. This method is applicable for the low heating rates and/or for the traps with the high attempt to escape frequencies, as it was in our case. An example of the fitting is presented in Fig. 8.

The superposition of the two Gaussian peaks with maxima located at 0.22 eV and 0.42 eV, respectively, is clearly seen in Fig. 6. The parameter σ, which describes the Gaussian distribution width, was 70-100 meV. These values coincide with the reported in literature [26].

The trapping state distribution depending on the exciting light spectral range was analyzed basing on the data presented in Fig. 4. The observed maxima amplitudes due to released charge carriers and their positions are influenced by the optical excitation below or above the band-gap. They are tending to saturate when quantum energy exceeds the band gap. Moreover, by increasing spectral width of the exciting light the curves are gradually flattening and the peak position is moving towards the lower temperatures, indicating

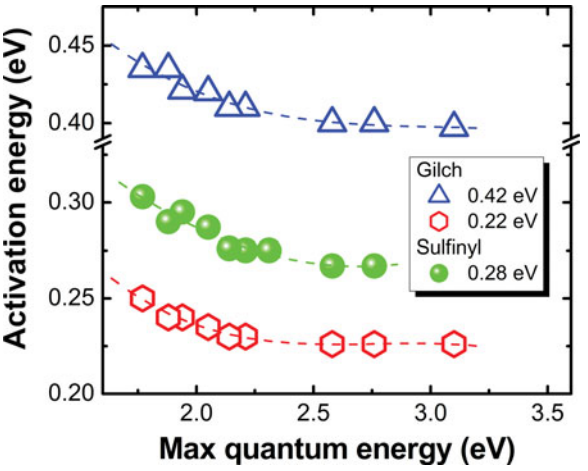

Figure 10. Effective activation energy depending on the exciting light spectral edge in the samples synthesized by the different routes as indicated on figure. The lines are eye-guides.

reduction of both the effective activation energy and the attempt to escape frequency. In Fig. 6a) two TSC peaks could be singled out, the first one being superimposed on the second. However, in the material synthesized by the Sulfinyl route TSC maximum at lower temperature was not present and the main maximum was located at lower temperature, as compared to that synthesized in the Gilch route.

The density of the filled trapping states N_t calculated from Eq. 2 is presented in Fig. 9 depending on the exciting light spectral edge. It can be seen that even if the light quanta energy is below the band gap a part of the traps becomes filled. This can be explained by the distribution of states of the band gap edges and that of the trapping states. In this case only the lowest states of the trapping levels will be filled, therefore their activation energy will be higher (Fig. 2). The trap filling and their effective activation energies tend to saturate when the quanta energy exceeds the band gap and absorption increases (Figs. 9 and 10).

The saturation values of the effective activation energy of traps are 0.22 eV and 0.40 eV for the Gilch route and 0.28 eV for the Sulphinyl one. They coincide with the data of MDMO-PPV[10] and MEH-PPV [27,28] obtained by TSC. Such activation energies were interpreted as caused by the hopping transport of carriers [29]. Moreover, TSC measurements with electrical trap filling showed the existence of percolation paths in the polymers [22]. However, polymer synthesized in the Sulfinyl route shows lower activation energies. The lower activation energy (0.28 eV) can be accompanied by an increase in the charge carrier life-time [13]. This implies that both polymers, though supposedly being identical in monomer-units, might indeed have different densities of the structural electronic defects that furthermore are characterized by the different effective activation energies. Sensitivity of other key transport parameters as, e.g., carrier mobility on the material structure was demonstrated also in, e.g., [11, 30, 31].

IV. Summary and Conclusions

MDMO-PPV conjugated polymers synthesized by the Gilch and Sulfinyl routes were investigated. A possibility of the direct evaluation of the trapping state energetical distribution by

the photo-thermo-electrical methods was demonstrated. The thermally stimulated currents were measured in the samples depending on the spectral range of the exciting light. By changing excitation spectral range the thermal activation energy values varied due to different filling of distributed in energy scale energy states. The Gaussian energy distribution of the trapping states was directly demonstrated by utilizing the repetitive heating technique. It was shown that two traps with the Gaussian distribution of the states and effective mean activation energies of about 0.22 and 0.40 eV are prevailing in the material synthesized in the Gilch route. Meanwhile 0.28 eV activation energy value was evaluated in MDMO-PPV produced according to the Sulfinyl route. The standard deviations of the distributions were evaluated to be 50–180 meV.

References

[1] So, F., & Kondakov, D. (2010). *Adv. Mater.*, *2*, 3762.
[2] Tsai, M., & Meng, H. (2005). *J. Appl. Phys.*, *97*, 114502.
[3] Goetz, S. M., Erlen, C. M., Grothe, H., Wolf, B., Lugli, P., & Scarpa, G. (2009). *Org. Electron.*, *10*, 573.
[4] Nikitenko, V. R., Kadashchuk, A., Schmechel, R., von Seggern, H., & Korosko, Yu. (2005). *J. Appl. Phys.*, *98*, 103702.
[5] Hartenstein, B., & Bässler, H. (1995). *J. Non-Cryst. Solids*, *190*, 112.
[6] Simmons, J. G., & Taylor, G. W. (1972). *Phys. Rev. B*, *5*, 1619.
[7] Bosacchi, A., Franchi, S., & Bosacchi, B. (1974). *Phys. Rev. B*, *10*, 5235.
[8] Chen, R. (1976). *J. Mat. Sci.*, *11*, 1521.
[9] Lewandowski, A. C., & Mc Keever, S. W. S. (1991). *Phys. Rev. B*, *43*, 8163.
[10] Kažukauskas, V., Čyras, V., Pranaitis, M., Apostoluk, A., Rocha, L., Sicot, L., Raimond, P., & Sentein, C. (2007). *Org. Electron.*, *8*, 21.
[11] Kažukauskas, V., Arlauskas, A., Pranaitis, M., Glatthaar, M., & Hinsch, A. (2010). *J. Nanosci. Nanotechnol.*, *10*, 1376.
[12] Brabec, C. J., Sariciftci, N. S., & Hummelen, J. C. (2001). *Adv. Funct. Mater.*, *11*, 15.
[13] Munters, T., Martens, T., Goris, L., Vrindts, V., Manca, J., Lutsen, L., De Ceuninck, W., Vanderzande, D., De Schepper, L., Gelan, J., Sariciftci, N. S., & Brabec, C. J. (2002). *Thin Solid Films*, *403–404*, 247.
[14] Cheng, Y. J., Yang, S. H., & Hsu, C. S. (2009). *Chem. Rev.*, *109*, 5868.
[15] Gilch, H. G., & Wheelwright, W. L. (1966). *J. Pol. Sci.*, *4*, 1337.
[16] Spreitzer, H., Becker, H., Kluge, E., Kreuder, W., Schenck, H., Demandt, R., & Schoo, H. (1998). *Adv. Mater.*, *10*, 1340.
[17] Louwet, F., Vanderzande, D., Gelan, J., & Mullens, J. (1995). *Macromolecules*, *28*, 1330.
[18] Louwet, F., Vanderzande, D., & Gelan, J. (1995). *Synth. Met.*, *52*, 125.
[19] Kuik, M., Vandenbergh, J., Goris, L., Begemann, E. J., Lutsen, L., Vanderzande, D. J. M., Manca, J. V., & Blom, P. W. M. (2011). *Appl. Phys. Lett.*, *99*, 183305.
[20] Sigma-Aldrich material data: http://www.sigmaaldrich.com/materials-science/organic-electronics/pcbm.html.
[21] Schwoerer, M., & Wolf, H. C. (2007). *Organic Molecular Solids*, Wiley-VCH: Weinheim.
[22] von Malm, N., Steiger, J., Heil, H., Schmechel, R., & von Seggern, H. (2002). *J. Appl. Phys.*, *92*, 7564.
[23] Pranaitis, M., Janonis, V., Sakavičius, A., & Kažukauskas, V. (2011). *Semicond. Sci. Tech.*, *26*, 085021.
[24] Grossweiner, L. I. (1953). *J. Appl. Phys.*, *24*, 1306.
[25] Hernandez, E., Duran, L., Durante Ricon, C. A., Aranguren, G., Guerrero, C., & Naranjo, J. (2002). *Cryst. Res. Technol.*, *37*, 1227.
[26] Bruting, W. (2005). *Physics of Organic Semiconductors*, Wiley-VCH: Weinheim.
[27] Kažukauskas, V., Tzeng, H., & Chen, S. A. (2002). *Appl. Phys. Lett.*, *80*, 2017.

[28] Kažukauskas, V. (2004). *Semicond. Sci. Technol.*, *19*, 1373.
[29] Townsend, P. D., & Friend, R. H. (1989). *Phys. Rev. B*, *40*, 3112.
[30] Kažukauskas, V., Pranaitis, M., Sicot, L., & Kajzar, F. (2006). *Mol. Cryst. Liq. Cryst.*, *447*, 459.
[31] Sentein, C., Rocha, L., Apostoluk, A., Raimond, P., Duyssens, I., Van Severen, I., Cleij, T., Lutsen, L., Vanderzande, D., Kažukauskas, V., Pranaitis, M., & Čyras, V. (2007). *Sol. En. Mat. Sol. Cells*, *91*, 1816.